[Article] www.whxb.pku.edu.cn

OH^-与CH_2ClF反应的阴离子产物通道

宋 磊[1] 于 锋[2] 吴琍霞[1] 周晓国[1,*] 刘世林[1]
([1]合肥微尺度物质科学国家实验室(筹), 中国科学技术大学化学物理系, 合肥 230026;
[2]西安工业大学数学物理系, 西安 710032)

摘要: 理论研究了羟基负离子(OH^-)与氟氯代甲烷(CH_2ClF)反应的阴离子产物通道. 分别在B3LYP/6-31+G(*d*,*p*)和B3LYP/6-311++G(2*d*,*p*)水平上得到反应势能面上各关键物种的优化构型, 进而计算得到谐振频率和零点能. 基于CCSD(T)/6-311+G(3*df*,3*dp*)水平的相对能量, 描述了由质子转移和双分子亲核取代(S_N2)过程生成各阴离子产物的途径. 各阴离子产物途径势垒的计算结果表明质子转移过程是实验中的主要产物通道, 与以往实验测量的结论相符. 此外, 计算还显示双分子亲核取代过程得到了非典型的阴离子产物, 其中动力学效应可能会导致F^-的生成.

关键词: 羟基负离子; 氟氯代甲烷; 反应机理; 质子转移; 亲核取代(S_N2)反应
中图分类号: O641

Anionic Production Pathways Involved in the Reaction between OH^- and CH_2ClF

SONG Lei[1] YU Feng[2] WU Li-Xia[1] ZHOU Xiao-Guo[1,*] LIU Shi-Lin[1]
([1]*Hefei National Laboratory for Physical Sciences at the Microscale, Department of Chemical Physics, University of Science and Technology of China, Hefei 230026, P. R. China*; [2]*Department of Mathematics and Physics, Xi′an Technological University, Xi′an 710032, P. R. China*)

Abstract: The anionic production pathways involved in the reaction between hydroxide anion (OH^-) and chlorofluoromethane (CH_2ClF) were theoretically investigated. The optimized geometries of all the important species on the reaction potential energy surface were obtained at the B3LYP/6-31+G(*d*,*p*) and B3LYP/6-311++G(2*d*,*p*) levels. Consequently, harmonic vibrational frequencies and zero point energies (ZPEs) were calculated. Based on the relative energies of all the species that were calculated at the CCSD(T)/6-311+G(3*df*,3*dp*) level, the anionic production channels for the H^+-abstraction and the bimolecular nucleophilic substitution (S_N2) reaction processes are elaborated upon. According to the calculated barrier heights for the production pathways, the H^+-abstraction channel is dominant, which agrees very well with previous experimental conclusions. In addition, non-typical anionic products are suggested to form during the S_N2 reaction processes where the serious dynamic effect probably causes the S_N2 reaction process to produce F^-.

Key Words: Hydroxide anion; Chlorofluoromethane; Reaction mechanism; Proton transfer; Nucleophilic substitution (S_N2) reaction

Received: November 24, 2010; Revised: January 24, 2011; Published on Web: March 2, 2011.

*Corresponding author. Email: xzhou@ustc.edu.cn; Tel: +86-551-3600031.

The project was supported by the National Natural Science Foundation of China (20603033, 10979042) and National Key Basic Research Program of China (973) (2007CB815204).
国家自然科学基金(20603033, 10979042)和国家重点基础研究发展规划(973) (2007CB815204)资助项目

1 Introduction

The reactions of anions with neutral molecules play an important role in ionospheric chemistry, organic chemistry, combustion chemistry, and surface chemistry,[1−3] thus the corresponding investigations have drawn extensive attention since 1950s. Many experimental techniques have been developed to explore these reactions in gas phase between anions with organic and inorganic molecules, such as flowing afterglow,[4] flow-drift tube,[5] ion cyclotron resonance,[6] tandem mass spectrum,[7] selected ion flow tube (SIFT),[8] and crossed beam.[9] The reaction rates and the branching ratios have been measured subsequently. Based on the observed products, the reaction mechanisms have been speculated. However, due to the influence of secondary reactions involved in experiments and low sensitivity of detectors, different experimental methods have always revealed very different reaction rate coefficients and branching ratios, e.g., the reported reaction rate coefficients and branching ratios are generally considered to be accurate to ±20%.[2,10] In addition, the electron detachment processes have been often involved in the reaction of anions with molecules, and the corresponding neutral products could not been probed by all aforementioned experimental techniques. Therefore, to uncover the comprehensive reaction mechanisms, theoretical calculations are believed to be more powerful to describe the reaction processes, especially when the secondary reactions and electron detachment channels exist.

Chlorofluorocarbons (CFCs) are considered to be accountable for the depletion of ozone and greenhouse effect.[11−13] Chlorofluoromethane (CH_2ClF) is a typical molecule of hydrochlorofluorocarbons (HCFCs),[14,15] which are formulated to be transitional replacements of the CFCs, used as refrigerants, solvents, blowing agents for plastic foam manufacture, and fire extinguishers under the Montreal Protocol.[16] However, since CH_2ClF includes chlorine atom as well, which is potentially released to do harm to the environment, some reactions[14,17−20] including the reactions of CH_2ClF with cations, anions, and OH radical have been investigated in both theoretical and experimental fields. Hydroxide anion (OH^-), as a typical nucleophile and base,[10,21] has active chemical properties like the atomic oxygen radical anion in the gas phase, and it can sink hazardous substances in the air by reacting with them. In addition, the comprehensive investigation of $OH^-(H_2O)_n$ with kinds of gas molecules has been thought to be able to provide a significant clue to liquid-phase reactions.[22,23] Therefore, it is meaningful to extensively study the OH^-+CH_2ClF reaction.

Mayhew *et al.*[10] have investigated the reaction of OH^- with CH_2ClF using the SIFT technique, and four potential thermodynamic production pathways have been probably involved as follows,

$$OH^- + CH_2ClF \begin{cases} \rightarrow CHClF^- + H_2O & H^+\text{-abstraction} \quad (1) \\ \rightarrow Cl^- + CH_2FOH & S_N2 \text{ with Cl} \quad (2) \\ \rightarrow F^- + CH_2ClOH & S_N2 \text{ with F} \quad (3) \\ \rightarrow OCl^- + CH_3F & \text{Cl-replacement} \quad (4) \end{cases}$$

These four pathways are defined as (1) proton abstraction, (2) S_N2 to produce Cl^-, (3) S_N2 to produce F^-, (4) replacement of Cl atom channel, respectively. Among these four production pathways, the channels (1−3) are exothermic, while the channel (4) is endothermic by 47 $kJ\cdot mol^{-1}$.[10] In Mayhew *et al.*′s experiment, only anionic products of channel (1) and (2) were observed as $CHClF^-$ (molar ratio, 90%) and Cl^- (molar ratio, 10%). No OCl^- anion from channel (4) was observed, which agrees with thermochemical surmise. However, the measured branching ratios of anionic products of $CHClF^-$ and Cl^- are on the contrary order to thermochemical results, and no F^- anions were observed although the channel (3) is exothermic as well. Thus, the extensive theoretical calculations are expected to reveal the detailed reaction mechanism and anionic production channels involved, and more information can be provided to deeply understand the S_N2 reaction pathway by comparing the channels (2) and (3). In addition, the theoretical calculations will also identify the neutral products, e.g., H_2+CHFO and/or $HF+CH_2O$ from channel (2), which cannot be revealed by the experiments yet.

In this work, the anionic production channels (1−3) involved in the title reaction will be investigated using quantum chemical calculations. Based on the calculated barrier heights for various production channels, the dominant production channel will be discussed, and thus the branching ratios observed in the previous experiments[10] will be explained.

2 Computational methods

All quantum chemical calculations were performed using the Gaussian 03 program package.[24] Geometries of all stationary points including reactants, intermediate complexes (IMs), transition states (TSs), and products on the potential energy surface (PES) were optimized at the B3LYP[25,26]/6-31+G(*d*,*p*) level. To consider the diffuse electron effects involved in the title reaction system, polarized and diffuse functions were expanded to the basis set, and the geometries were re-optimized at the B3LYP/6-311++G(2*d*,*p*) level to study the expansive basis set effects. Harmonic vibrational frequencies, ZPEs (scaled by a factor of 0.9857),[27] and thermal enthalpy corrections were calculated at the B3LYP/6-31+G(*d*,*p*) level. Moreover, intrinsic reaction coordinate (IRC)[28,29] calculations at the B3LYP/6-31+G(*d*,*p*) level were performed to identify the corresponding reactant and product for every transition state. The Mulliken population analysis[30] was utilized to characterize the charge distributions for the intermediate complexes and anionic products. The single point energies of stationary points were calculated at the CCSD(T)[31−33]/6-311+G(3*df*,3*dp*) level with the B3LYP/6-31+G(*d*,*p*) optimized geometries, and subsequently the relative energies were obtained as well as reaction enthalpies. To compare with the experimental data, the reaction enthalpies at the CCSD(T)/aug-cc-pVDZ and G3MP2B3[34,35] levels were also calculated to verify the reliability of the present calculated results at the CCSD(T)/6-311+G(3*df*,3*dp*) level.

3 Results and discussion

The reaction enthalpies at 298.15 K of the production channels (1–3) were calculated at the G3MP2B3, CCSD(T)/aug-cc-pVDZ, and CCSD(T)/6-311+G(3*df*,3*dp*) levels, respectively, and listed in Table 1, where all calculated enthalpies have already included the thermal correction at the B3LYP/6-31+G(*d*, *p*) level. Although our previous calculations on the similar reaction systems, e.g., $O^-+C_2H_4$,[36,37] $O^-+C_5H_5N$,[38] O^-+CH_3CN,[39] exhibited the most accurate relative energies obtained at the G3MP2B3 level, the CCSD(T)/6-311+G(3*df*,3*dp*) level shows the best performance in the title reaction, and the maximum error is within 3 kJ·mol^{-1}. The potential reason is due to the difference between the open-shell and close-shell systems.

As we expected, all final products of channels (1–3) could be produced through a typical multi-step reaction process as shown in the following schemes.

$$OH^- + CH_2ClF \rightarrow IM1 \begin{cases} \xrightarrow{TS1} IM2 \rightarrow CHClF^- + H_2O \\ \xrightarrow{TS2} IM3 \rightarrow CH_2FOH + Cl^- \\ \xrightarrow{TS5} IM5 \rightarrow CH_2FOH + Cl^- \\ \xrightarrow{TS5} CH_2ClOH + F^- \end{cases} \quad (5)$$

where the CH_2FOH fragment could further dissociate to CHFO+H_2 or CH_2O + HF. Fig.1 shows the optimized geometries of main reactants, products, IMs and TSs, where parameters in normal type were obtained at the B3LYP/6-31+G(*d*,*p*) level and those in bold type were calculated at the B3LYP/6-311++G(2*d*,*p*) level. Briefly, all geometry parameters at both levels are consistent, and the differences of bond length and bond angles are less than 0.0032 nm and 1.6°. Therefore, the diffuse electron effect is not serious in the title reaction, although some molecular structures are very loose. Thus the B3LYP/6-31+G(*d*,*p*) geometries are used in the following sections unless otherwise noted.

The CCSD(T)/6-311+G(3*df*,3*dp*) relative energies at 0 K with ZPEs correction of all species involved in the title reaction are summarized in Table 2, where the imaginary frequencies of transition states calculated at the B3LYP/6-31+G(*d*,*p*) level are listed as well. Based on these relative energies, the potential energy profile of the title reaction is shown in Fig.2, where the anionic production pathways (1–3) are represented respectively.

On the entrance PES of the title reaction, a unique intermediate complex denoted by IM1 is formed rapidly with OH^- approaching CH_2ClF, due to the ion-induced dipole interaction. As shown in Fig.1, the bond length of active C—H bond is elongated from 0.1090 nm in the CH_2ClF to 0.1157 nm in IM1, and the distance between approaching OH^- and the active H atom is 0.1595 nm, even much shorter than a normal hydrogen bonding length, indicating that the ion-induced dipole interaction is very strong indeed. The energy of IM1 is 96.8 kJ·mol^{-1} lower than those of reactants, thus it can further isomerize and dissociate to final products. As mentioned above, there are three anionic production channels (1–3) probably involved in the reaction, which will be described in the following processes, e.g., H^+-abstraction and S_N2 reactions.

Table 1 Reaction enthalpies (in kJ·mol^{-1}) of various production channels at 298.15 K

Channel	G3MP2B3[a]	CCSD(T)/ aug-cc-pVDZ	CCSD(T)/ 6-311+G(3*df*,3*dp*)	Experiment[10]
$CHClF^-+H_2O$	−29.8	−26.2	−20.9	−18
Cl^-+CH_2FOH	−273.3	−259.9	−261.2	−261
F^-+CH_2ClOH	−98.3	−102.1	−94.5	

[a] The standard 6-31G(*d*) basis set is replaced by the 6-31+G(*d*,*p*) basis set when geometries are optimized in G3MP2B3 method.

3.1 H^+-abstraction reaction channel (1)

IM1 can isomerize to IM2 through TS1 with a very lower barrier. As shown in Fig.1, the structures of IM1, TS1, and IM2 are fairly similar, in which the structure of CHFCl moiety is almost kept and only the distances between O and active H atom, C and the H atom are changed dramatically. The distance of O and H atom is shortened from 0.1595 nm in IM1 to 0.1274 nm in TS1, followed by a decrease to 0.1036 nm in IM2, while the C—H bond length is elongated gradually from 0.1157 nm in IM1 to 0.1343 nm in TS1 and 0.1772 nm in IM2. Thus, the O—H bond is formed and the C—H bond is broken in this isomerization process. Meanwhile, the producing H—O—H angle decreases to 102.87° in IM2, implying a water molecule is formed actually in IM2. Obviously, IM2 is an ion-induced dipole complex of $CHFCl^-$ and H_2O, and thus it can decompose to the final products, H_2O and $CHClF^-$, by collision-induced dissociation without barriers. The overall production pathway is exothermic by 23.2 kJ·mol^{-1}.

The present IRC calculations confirm that TS1 is the isomerization barrier from IM1 to IM2 indeed. The minimum energy path at the B3LYP/6-31+G(*d*,*p*) level along this process is shown in Fig.3, where the charge distributions are obtained by the Mulliken population analysis and represented as well. A typical electron transfer happens in this process, and the negative charge of OH^- anion is almost completely transferred to the CHFCl moiety in the transition state region. As a result, the produced intermediate IM2 is a complex of $CHFCl^-$ and H_2O indeed.

The similar phenomena were observed in the reaction of OH^- with $CH_{(4-n)}Cl_n$ (n=1–4) by Borisov *et al*.[40] As they mentioned, the barrier heights of H^+-abstraction decrease with the increasing of n (n=1–4), and moreover, these barriers even vanish away when the n equals to 3 or over. Actually, this change tendency of barrier height is related to the acidity of protons on halogens and the alkalinity of OH^-. With the increasing of the number of halogens, the protons become more and more acidic, and thus the H^+-abstraction more probably proceeds.

3.2 S_N2 reaction channel to produce Cl^- (2)

The S_N2 reaction pathway to produce Cl^- also starts from IM1. As shown in Fig.2, this process passes a barrier and produces a complex on the exit PES. The overall reaction pathway is similar to the reaction of OH^- with CH_2F_2.[41]

The transition state has the $[HO\cdots CH_2F\cdots Cl]^-$ structure of

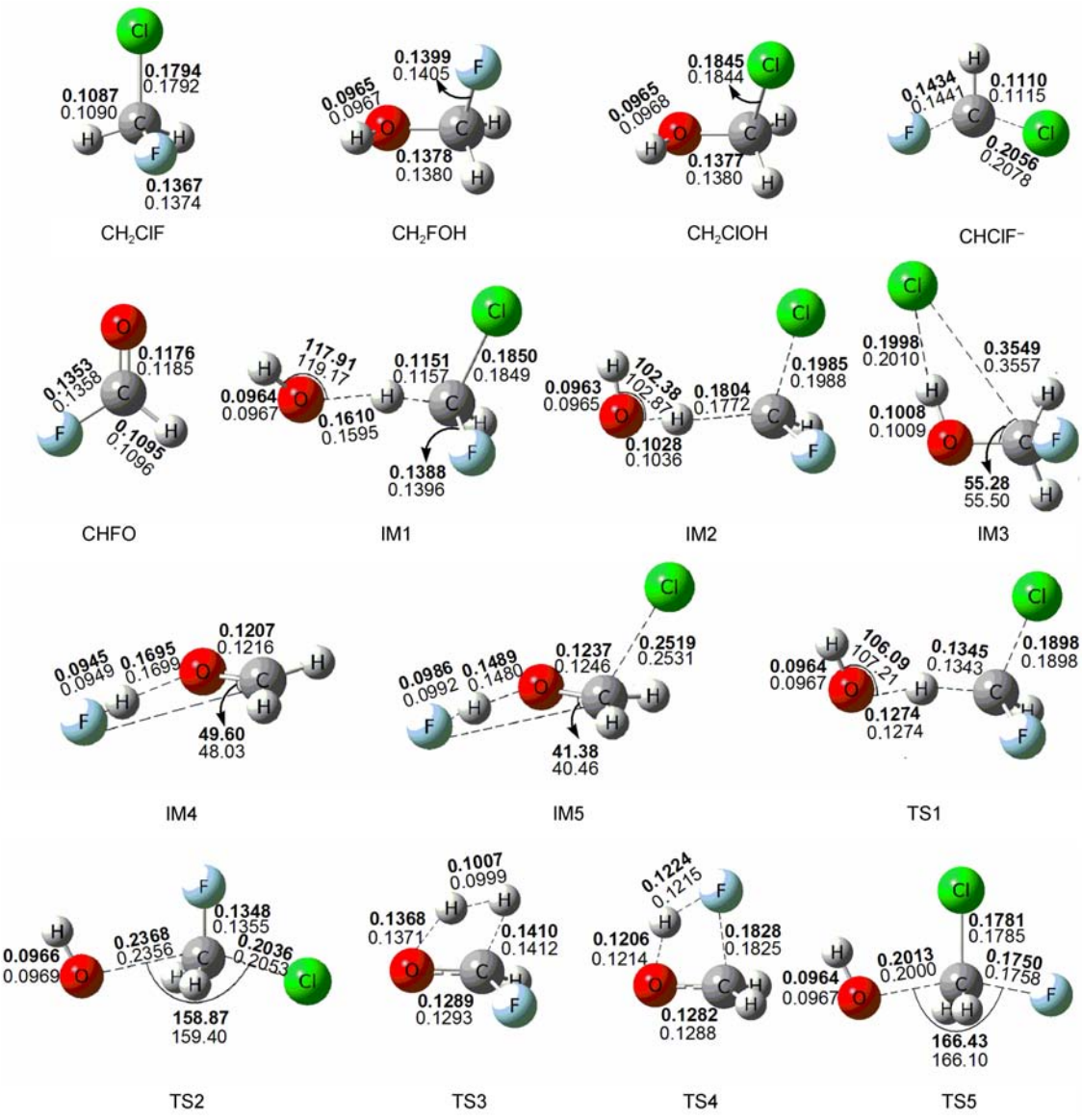

Fig.1 Optimized geometries of main reactants, products, intermediate complexes (IMs) and transition states (TSs) of the title reaction

Bond lengths are in nm, and bond angles are in degree. The parameters in normal type are the geometric parameters optimized at the B3LYP/6-31+G(*d*,*p*) level, while those in bold type stand for the geometric parameters optimized at the B3LYP/6-311++G(2*d*,*p*) level.

C_s symmetry and is noted as TS2. As shown in Fig.1, the C—Cl bond length is elongated from 0.1849 nm in IM1 to 0.2053 nm in TS2, while the distance between C and O atoms is shortened to 0.2356 nm in TS2. Three atoms (O, C, and Cl) are nearly collinear. Therefore, this transition state looks very like a typical S_N2 reaction transition state, which should connect to a collinear product-like complex of $CH_2FOH\cdots Cl^-$ structure on the exit PES. However, the forward IRC calculation indicates that an unexpected potential minimum $CH_2FOH\cdots Cl^-$ (denoted by IM3) will be formed. IM3 breaks the C_s symmetry of the S_N2 reaction system and is not the traditional collinear S_N2 product complex. As indicated in Fig.4, there is a special exit-channel stage along MEP, which is noted as CX1. The relative energy along MEP dramatically drops to CX1 on the first stage after TS2, and then decreases slowly. The structure of CX1 looks very like the expected collinear S_N2 product complex ($Cl^-\cdots CH_2FOH$), although it is not a real potential minimum. Actually, the dissociating Cl^- will roam towards the CH_2FOH moiety and abstract the proton of OH group, due to the strong ion-induced dipole interaction. Thus the collinear symmetry is broken and a hydrogen-bond between H and Cl atoms is formed to be 0.2010 nm in IM3. In addition, the negative charge of OH^- anion is transferred to the Cl atom in the transition state region as shown in Fig.4. Thus the produced intermediate IM3 is a complex of Cl^- and CH_2FOH indeed.

The energy of TS2 is 32.2 kJ·mol^{-1} higher than that of IM1, and the energy difference between TS2 and IM3 is 282.2 kJ·mol^{-1}. Thus it is highly exothermic from IM1 to IM3, and IM3 is energetic enough to proceed subsequent decomposition and isomerization. As shown in Fig.2, IM3 can decompose easily

Table 2 Total energies and relative energies at 0 K, enthalpies at 298.15 K of all species involved in the title reaction calculated at the CCSD(T)/6-311+G(3*df*,3*dp*) level with ZPEs correction and enthalpies correction, respectively

Species	Imaginary frequency/cm^{-1} [a]	ZPE/hartree	E_0/hartree	ΔE/(kJ·mol^{-1})	ΔH(298.15 K)/(kJ·mol^{-1})[c]
$CH_2ClF+OH^-$		0.03899	−674.34836	0	0
$CHClF^-+H_2O$		0.03593	−674.35720	−23.2	−20.9
$CH_2ClOH+F^-$		0.04280	−674.38138	−86.7	−94.6
$CH_2FOH+Cl^-$		0.04431	−674.44463	−252.8	−261.2
$CHFO+H_2+Cl^-$		0.03050	−674.43077	−216.4	217.3
$CH_2O+HF+Cl^-$		0.03542	−674.43170	−218.8	−220.2
IM1		0.03889	−674.38524	−96.8	−97.4
IM2		0.03880	−674.38567	−98.0	−98.3
IM3		0.04457	−674.48044	−346.8	−350.5
IM4 + Cl^-		0.03926	−674.44163	−244.9	−249.6
IM5		0.04104	−674.47155	−323.4	−325.1
TS1	845i	0.03529	−674.38544	−97.4	−99.2
TS2	210i	0.03964	−674.37297	−64.6	−66.5
TS3+Cl^-	2237i [b]	0.03495	−674.30980	101.2	92.4
TS4+Cl^-	1696i[b]	0.03620	−674.37397	−67.2	−75.4
TS5	549i	0.03975	−674.35294	−12.0	−14.7

[a] Imaginary frequencies are calculated at the B3LYP/6-31+G(*d*,*p*) level; [b]Imaginary frequencies listed here are for TS3 and TS4, respectively; [c]ΔE and ΔH(298.15 K) are corrected respectively with ZPEs correction and enthalpies correction, which are calculated with the scaled vibrational frequencies (scaled factor is 0.9857) at the B3LYP/6-31+G(*d*,*p*) level.

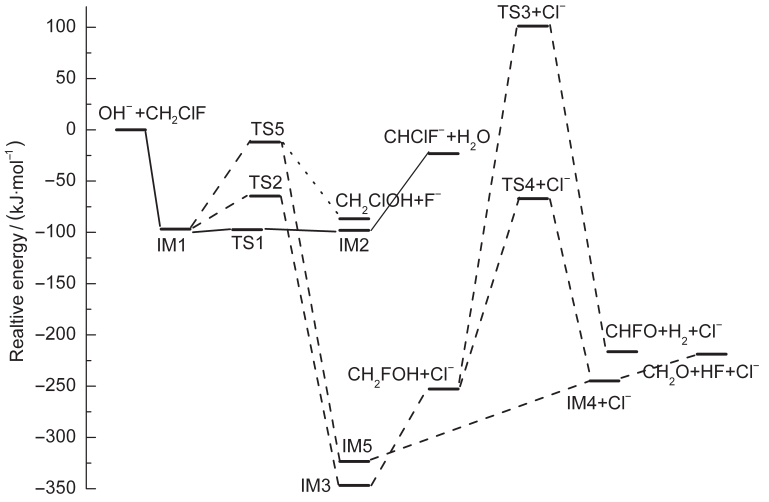

Fig.2 Schematic diagram of the relative energies of various species on the reaction PES at the CCSD(T)/6-311+G(3*df*,3*dp*) level

to Cl^- and CH_2FOH directly, and the overall reaction pathway of $OH^-+CH_2FCl \rightarrow Cl^-+CH_2FOH$ is exothermic by 252.8 kJ·mol^{-1}. However, CH_2FOH cannot exist stably, and further dissociations will take place to produce H_2 + CHFO and/or HF + CH_2O. The corresponding TSs are denoted as TS3 and TS4, respectively. As shown in Table 1, the total energy of TS3 and Cl^- is 101.2 kJ·mol^{-1} higher than that of reactants, and thus this pathway to produce H_2 and CHFO is difficult to happen in experiment. On the contrary, although the channel to produce HF and CH_2O also needs overcome a high barrier (TS4) of 185.6 kJ·mol^{-1}, the energy of TS4+Cl^- is still lower than that of reactants. Therefore HF and CH_2O should be the real neutral products corresponding to Cl^- observed in experiment.

3.3 S_N2 reaction channel to produce F^- (3)

The other S_N2 reaction process of the title reaction is expected to produce F^- and CH_2ClOH *via* isomerization and decomposition of IM1. As shown in Fig.1, a transition state with the $[HO\cdots CH_2Cl\cdots F]^-$ structure and C_s symmetry is found and denoted as TS5. Obviously, TS5 is rather similar to TS2 which is a traditional S_N2 transition state to produce F^-, where the C—F bond length is elongated from 0.1396 nm in IM1 to 0.1758 nm in TS5, and the distance between C and O atoms is shortened to 0.2000 nm in TS5. To our surprise, the forward IRC calculation of TS5 points to an unexpected potential minimum IM5 instead of the S_N2 reaction product $F^-\cdots CH_2ClOH$. As shown in Fig.5, IM5 is nearly a three-body intermediate complex of

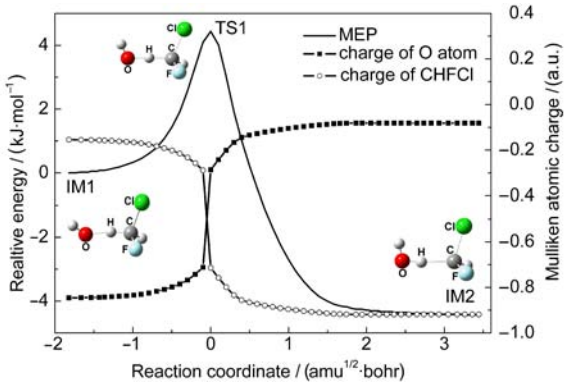

Fig.3 The minimum energy path (MEP) at the B3LYP/6-31+G(*d*,*p*) level along the isomerization process from IM1 to IM2

The charge distributions of O atom and CHFCl moiety are also shown.

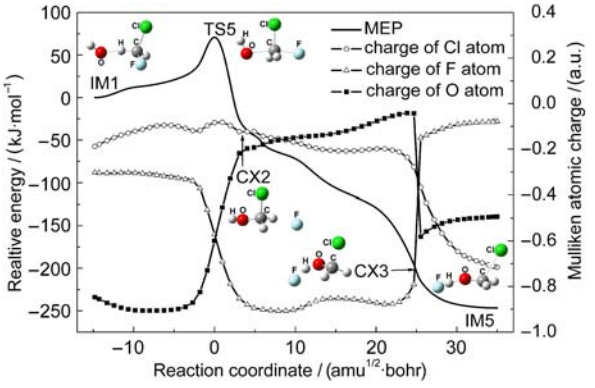

Fig.5 The minimum energy path at the B3LYP/6-31+G(*d*,*p*) level along the reaction process from IM1 to IM5

The charge distributions of O, Cl and F atoms are shown as well.

$Cl^-\cdots CH_2O\cdots HF$, where the $CH_2O\cdots HF$ moiety is very similar to IM4 and a much stronger hydrogen bond of 0.1480 nm exists between the HF and O atom. Thus, IM5 can subsequently dissociate to Cl^-, CH_2O and HF by collision without any barrier.

The detailed information of geometry and charge distributions in this process is exhibited in Fig.5. Along MEP, the initial reaction stage after TS5 undergoes a typical S_N2 process and the relative energy quickly drops, and a S_N2 product complex ($F^-\cdots CH_2ClOH$) is formed (denoted as CX2 in Fig.5). However, because CX2 is not a real potential minimum, the energy drops forward slowly on the PES. Due to the strong ion-induced dipole interaction, the dissociating F^- will roam towards the CH_2ClOH moiety and abstract a proton of OH group. Thus, HF and formaldehyde (CH_2O) are produced, and Cl^- is repulsed far away. A strong hydrogen-bond between F and O connects the HF and CH_2O molecules. A complex CX3 is noted in Fig.5 and represents this special stage on PES. As shown in Fig.5, the negative charge of OH^- anion is transferred to the F atom initially in the region of TS5, while the electron is re-exchanged when the F^- extracts a proton of OH group to produce HF and formaldehyde in the CX3 region. Thus IM5 replaces the expected S_N2 reaction product and is finally produced along the MEP.

Here we should demonstrate that all mentioned MEPs related to TS2 and TS5 only reflect static reaction pathways, and dynamic effects probably exist prominently in the anion-molecule reaction[42–46] especially for the S_N2 reaction channels, e.g., the S_N2 reaction products of F^-+CH_3O are confirmed to occur along the dynamic reaction pathway in the O^-+CH_3F reaction, although the static reaction process related to the corresponding S_N2 transition state does point to other products of HF + CH_2O^-. Since geometries of the S_N2 transition states and MEPs for the title reaction and O^-+CH_3F reaction are very similar, the S_N2 reaction channel (3) to produce F^- and CH_2ClOH can also be expected to happen in a real experiment, as well as the Cl^- + CH_2O + HF production pathway. However, due to the much higher energy of TS5 than that of TS2, the branching ratio of anionic products from the S_N2 channel (3) are minor indeed. Therefore, for both S_N2 reaction processes (2) and (3), the dominant products should be Cl^-, HF, and formaldehyde.

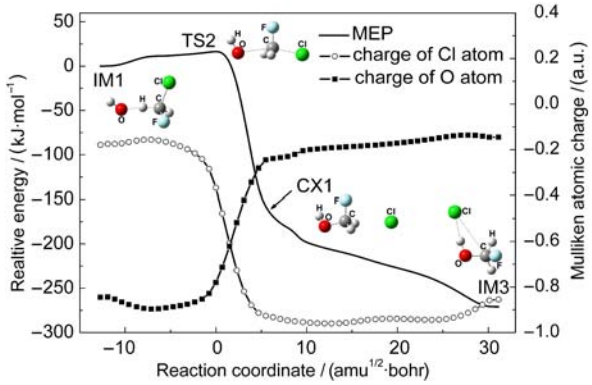

Fig.4 The minimum energy path at the B3LYP/6-31+G(*d*,*p*) level along the isomerization process from IM1 to IM3

The charge distributions of O and Cl atoms are shown as well.

3.4 Comparisons with the previous experimental conclusions

Based on the calculated barrier heights and reaction enthalpies, the H^+-abstraction (1), S_N2 reaction channels (2) and (3) can take place and the Cl^- and $CHClF^-$ anions are expected to produce, which is consistent with the observed anionic products in experiments.[10] In addition, all three anionic production channels pass the same initial intermediate complex IM1 on the entrance PES, and thus the branching ratios should mainly depend on the barrier heights of subsequent isomerization and decomposition processes. Since the transition state TS1 has the lowest relative energy compared with TS2 and TS5, the H^+-abstraction channel (1) is dominant, which agrees well with the experimental conclusions.[10]

4 Conclusions

The anionic production pathways involved in the reaction of hydroxide anion (OH^-) with chlorofluoromethane (CH_2ClF) have been studied. The unique intermediate has been located on the entrance potential energy surface, which is a typical ion-induced dipole complex indeed. All anionic products are formed *via* the isomerization and decomposition of this intermediate.

Based on the calculated barrier heights and reaction enthalpies, the H^+-abstraction and two S_N2 reaction channels can take place, and thus the Cl^- and $CHClF^-$ anions are expected to produce finally, which is consistent with the observed anionic products in experiments. Since the transition state of H^+-abstraction process has the lowest barrier height compared with those of the S_N2 reaction channels, the H^+-abstraction channel is certainly dominant, which agrees well with the experimental conclusions. In addition, present calculation also shows that the major neutral molecule products corresponding to the S_N2 channel to produce Cl^- should be HF and formaldehyde. Moreover, the MEP revealed by IRC calculations of the S_N2 channel of OH^- attacking C—F bond of CH_2FCl represents the static reaction pathway to produce Cl^- instead of the S_N2 reaction product F^-, however the characteristics of MEP imply that probably the serious dynamic effect exists in the real reaction process. As a result, the dynamic S_N2 reaction process to produce F^- probably happens in experiment, and the further trajectory calculations are undergoing to confirm our prediction.

Acknowledgments: Authors are grateful to Supercomputing Center of University of Science and Technology of China (USTC) for the computational resources support of this work.

References

(1) Deckers, J.; van Tiggelen, A. *Combust. Flame* **1957,** *1*, 281.
(2) Lee, J.; Grabowski, J. J. *Chem. Rev.* **1992,** *92*, 1611.
(3) Fialkov, A. B. *Prog. Energy Combust. Sci.* **1997,** *23*, 399.
(4) Grabowski, J. J.; Melly, S. J. *Int. J. Mass Spectrom.* **1987,** *81*, 147.
(5) McFarland, M.; Albritton, D. L.; Fehsenfeld, F. C.; Ferguson, E. E.; Schmeltekopf, A. L. *J. Chem. Phys.* **1973,** *59*, 6610.
(6) Beauchamp, J. L. *Annu. Rev. Phys. Chem.* **1971,** *22*, 527.
(7) Futrell, J. H.; Miller, C. D. *Rev. Sci. Instrum.* **1966,** *37*, 1521.
(8) Adams, N. G.; Smith, D. *Int. J. Mass Spectrom. Ion Phys.* **1976,** *21*, 349.
(9) Bilotta, R. M.; Preuninger, F. N.; Farrar, J. M. *J. Chem. Phys.* **1980,** *73*, 1637.
(10) Mayhew, C. A.; Peverall, R.; Timperley, C. M.; Watts, P. *Int. J. Mass Spectrom.* **2004,** *233*, 155.
(11) Solomon, S. *Rev. Geophys.* **1999,** *37*, 275.
(12) Rowland, F. S. *Ambio* **1990,** *19*, 281.
(13) Molina, M. J.; Rowland, F. S. *Nature* **1974,** *249*, 810.
(14) Bhatnagar, A.; Carr, R. W. *Chem. Phys. Lett.* **1996,** *258*, 651.
(15) Blanco, S.; Lesarri, A.; López, J. C.; Alonso, J. L.; Guarnieri, A. *J. Mol. Spectrosc.* **1995,** *174*, 397.
(16) http://en.wikipedia.org/wiki/Montreal_Protocol (accessed May 4, 2010).
(17) Howle, C. R.; Mayhew, C. A.; Tuckett, R. P. *J. Phys. Chem. A* **2005,** *109*, 3626.
(18) Peverall, R.; Kennedy, R. A.; Mayhew, C. A.; Watts, P. *Int. J. Mass Spectrom.* **1997,** *171*, 51.
(19) Chiorboli, C.; Piazza, R.; Tosato, M. L.; Carassiti, V. *Coord. Chem. Rev.* **1993,** *125*, 241.
(20) Bottoni, A.; Poggi, G.; Emmi, S. S. *J. Mol. Struct. -Theochem* **1993,** *279*, 299.
(21) Tanner, S. D.; Mackay, G. I.; Bohme, D. K. *Can. J. Chem.* **1981,** *59*, 1615.
(22) Yang, X.; Zhang, X.; Castleman, A. W. *J. Phys. Chem.* **1991,** *95*, 8520.
(23) Yang, X.; Castleman, A. W. *J. Am. Chem. Soc.* **1991,** *113*, 6766.
(24) Frisch, M. J.; Trucks, G. W.; Schlegel, H. B.; *et al*. *Gaussian 03,* Revision C.02, D.01, E.01; Gaussian Inc.: Pittsburgh, PA, 2003.
(25) Lee, C.; Yang, W.; Parr, R. G. *Phys. Rev. B* **1988,** *37*, 785.
(26) Becke, A. D. *J. Chem. Phys.* **1993,** *98*, 1372.
(27) Merrick, J. P.; Moran, D.; Radom, L. *J. Phys. Chem. A* **2007,** *111*, 11683.
(28) Gonzalez, C.; Schlegel, H. B. *J. Phys. Chem.* **1990,** *94*, 5523.
(29) Gonzalez, C.; Schlegel, H. B. *J. Chem. Phys.* **1989,** *90*, 2154.
(30) Mulliken, R. S. *J. Chem. Phys.* **1955,** *23*, 1833.
(31) Purvis, G. D.; Bartlett, R. J. *J. Chem. Phys.* **1982,** *76*, 1910.
(32) Urban, M.; Noga, J.; Cole, S. J.; Bartlett, R. J. *J. Chem. Phys.* **1985,** *83*, 4041.
(33) Scuseria, G. E.; Janssen, C. L.; Schaefer, H. F. *J. Chem. Phys.* **1988,** *89*, 7382.
(34) Curtiss, L. A.; Redfern, P. C.; Raghavachari, K.; Rassolov, V.; Pople, J. A. *J. Chem. Phys.* **1999,** *110*, 4703.
(35) Baboul, A. G.; Curtiss, L. A.; Redfern, P. C.; Raghavachari, K. *J. Chem. Phys.* **1999,** *110*, 7650.
(36) Yu, F.; Zhao, Y. G.; Wang, Y.; Zhou, X. G.; Liu, S. L. *Acta Chim. Sin.* **2007,** *65*, 899. [于 锋, 赵英国, 王 勇, 周晓国, 刘世林. 化学学报, **2007,** *65*, 899.]
(37) Wang, X. L.; Yu, F.; Xie, D.; Liu, S. L.; Zhou, X. G. *Acta Chim. Sin.* **2008,** *66*, 2499. [王新磊, 于 锋, 谢 丹, 刘世林, 周晓国. 化学学报, **2008,** *66*, 2499.]
(38) Wu, L. X.; Yu, F.; Song, L.; Zhou, X. G.; Liu, S. L. *J. Mol. Struct. -Theochem* **2010,** *958*, 82.
(39) Yu, F.; Wu, L. X.; Zhou, X. G.; Liu, S. L. *Chin. J. Chem. Phys.* **2010,** *23*, 643. [于 锋, 吴琍霞, 周晓国, 刘世林. 化学物理学报, **2010,** *23*, 643.]
(40) Borisov, Y. A.; Arcia, E. E.; Mielke, S. L.; Garrett, B. C.; Dunning, T. H. *J. Phys. Chem. A* **2001,** *105*, 7724.
(41) Lee, E. P. F.; Dyke, J. M.; Mayhew, C. A. *J. Phys. Chem. A* **1998,** *102*, 8349.
(42) Yu, F.; Wu, L. X.; Song, L.; Zhou, X. G.; Liu, S. L. *J. Mol. Struct. -Theochem* **2010,** *958*, 41.
(43) Yu, F.; Wu, L. X.; Liu, S. L.; Zhou, X. G. *J. Mol. Struct. -Theochem* **2010,** *947*, 1.
(44) Wu, L. X.; Yu, F.; Liu, J.; Dai, J. H.; Zhou, X. G.; Liu, S. L. *Acta Phys. -Chim. Sin.* **2010,** *26*, 2331. [吴琍霞, 于 锋, 刘 静, 戴静华, 周晓国, 刘世林. 物理化学学报, **2010,** *26*, 2331.]
(45) Sun, L.; Song, K.; Hase, W. L. *Science* **2002,** *296*, 875.
(46) Hase, W. L. *Science* **1994,** *266*, 998.